Aerosol Science and Technology, 43:486–501, 2009

ISSN: 0278-6826 print / 1521-7388 online
DOI: 10.1080/02786820902763132

Measurement of Aerosol Organic Compounds Using a Novel Collection/Thermal-Desorption PTR-ITMS Instrument

Troy Thornberry,[1,2] Daniel M. Murphy,[1] David S. Thomson,[1,2] Joost de Gouw,[1,2] Carsten Warneke,[1,2] Timothy S. Bates,[3] Patricia K. Quinn,[3] and Derek Coffman[3]

[1]*NOAA Earth System Research Laboratory, Chemical Science Division, Boulder, Colorado, USA*
[2]*Cooperative Institute for Research in Environmental Sciences, University of Colorado, Boulder, Colorado, USA*
[3]*NOAA Pacific Marine Environmental Laboratory, Seattle, Washington, USA*

We report the development and characterization of a proton-transfer-reaction ion trap mass spectrometer for the speciated measurement of organic compounds in atmospheric aerosols and show results from its first field deployment. The instrument uses an aerosol collection inlet to accumulate aerosol mass followed by rapid thermal desorption to volatilize the organic compounds for in situ analysis. We have performed laboratory studies to characterize instrument performance and the instrument was deployed aboard a NOAA research vessel during the Texas Air Quality Study 2006/Gulf of Mexico Atmospheric Composition and Climate Study (TexAQS 2006/GoMACCS) in August–September 2006. The laboratory-determined detection limit for glutaric acid in mixed glutaric acid/NH_4HSO_4 test aerosols was 0.22 ng collected mass, which corresponds to an estimated detection limit of 12 ng m^{-3} for a 10 min sample based on the instrument sample flow rate of 1.8 L min^{-1}. During TexAQS 2006/GoMACCS, signals well above the detection limit were observed at a number of mass to charge ratios, mostly occurring during an extended period of active pollution photochemistry, but also including detection of possible primary emissions of aerosol-phase pyridine.

INTRODUCTION

Organic compounds comprise a significant and highly variable fraction of tropospheric aerosol (Penner et al. 2001; Seinfeld and Pankow 2003; Zhang et al. 2007) and affect the optical and microphysical properties of aerosols (Kanakidou et al. 2005). Hundreds to thousands of individual organic compounds have been observed in atmospheric aerosols (Hamilton et al. 2004). Some aerosol organic compounds are directly emitted (primary organic aerosol, POA), while others are produced through chemical reactions in the atmosphere (secondary organic aerosol, SOA).

There has also been recent evidence from chamber studies and ambient samples that oligomerization and polymerization reactions occur in aerosols (Kalberer et al. 2004), which could lead to the incorporation of volatile organic compounds (VOCs), such as glyoxal into the aerosol phase (Volkamer et al. 2007).

Models of the evolution of organic aerosol mass using laboratory-determined SOA yields and measured VOC mixing ratios have consistently underpredicted the organic aerosol mass fraction when compared to measurements in a number of recent field campaigns (de Gouw et al. 2005; Volkamer et al. 2006; de Gouw et al. 2008; Kleinman et al. 2008), leading to efforts to explain the missing source of aerosol organics. One potential source of additional organic aerosol mass is semivolatile species that partition between the gas and aerosol phases, but are not observed by standard VOC and nonvolatile-OC measurement techniques (Donahue et al. 2006; Robinson et al. 2007).

The nature of aerosol organic compounds and how they change with time are important in understanding the properties of aerosols, but detailed knowledge of the composition of the organic fraction of atmospheric aerosols remains limited (Fuzzi et al. 2006).

Historically, measurements of aerosol organic composition have typically involved long sampling periods (hours to days) using high volume filter samplers followed by solvent extraction of the collected material, and often derivatization, before analysis. Most of these methods still only resolve a portion of the organic mass (e.g., the water soluble fraction) or focus on certain classes of compounds (Seinfeld and Pankow 2003). This continues to be the most common method for regular determination of aerosol organic species.

The need to characterize the variability in aerosol composition in space and time has led to the development of new

Received 8 October 2008; accepted 15 January 2009.
This work was supported by the NOAA Climate and Global Change Program. The authors gratefully acknowledge the assistance of Drew Hamilton and the officers and crew of NOAA Ship *Ronald H. Brown* during the deployment for the TexAQS 2006/GoMACCS cruise.
Address correspondence to Troy Thornberry, NOAA Earth System Research Laboratory, 325 Broadway R/CSD6, Boulder, CO 80305, USA. E-mail: troy.thornberry@noaa.gov

measurement techniques that have significantly increased spatial and temporal resolution, but often at the expense of specificity. Instruments such as PALMS (Murphy and Thomson 1995) and ATOFMS (Prather et al. 1994) are able to qualitatively determine the composition of single aerosol particles; however, the laser ablation/ionization analysis technique results in significant fragmentation of organic molecules into common organic fragments and does not typically allow determination of individual organic species. The Aerodyne Aerosol Mass Spectrometer (AMS) (Jayne et al. 2000; Canagaratna et al. 2007) uses thermal ablation and electron impact ionization mass spectrometry to make a quantitative measurement of non-refractory aerosol composition and can report total organic mass and various proxies for the degree of oxidation of the organics (Zhang et al. 2005), including recent measurements of the O/C ratio present in the aerosol organic fraction (Aiken et al. 2008). This method, however, results in significant fragmentation of organic compounds and typically precludes speciation. Oktem et al. (2004) reported a new instrument to measure aerosol organics using a particle collection/IR photodesorption/VUV photoionization/TOF mass spectrometry approach (PIAMS), which resulted in considerably less fragmentation of organic species than electron impact. La Franchi and Petrucci (2006) describe an instrument using aerosol collection/thermal desorption coupled with photoelectron resonance capture ionization/TOF mass spectrometry (PERCI) to detect individual organic species in aerosols. Another recent approach is the use of aerosol collection/thermal desorption coupled to GC/MS analysis (TAG) reported by Williams et al. (2006).

Chemical ionization mass spectrometry (CIMS) has been used in laboratory and field applications for measurement of many gas-phase species, including OH (Eisele and Tanner 1991), H_2SO_4 (Eisele and Tanner 1993), HNO_3 (Huey et al. 1998), NH_3 (Nowak et al. 2002), and various organic compounds (Lindinger et al. 1998; Slusher et al. 2004; de Gouw and Warneke 2007; Huey 2007). Advantages of CIMS include the possibility for selective ion-molecule chemistry and relatively non-fragmentative ionization. Application of CIMS for the measurement of aerosol organic compounds has also recently been reported for laboratory and chamber experiments (Hearn and Smith 2004; Hearn and Smith 2006) and for the analysis of nucleation mode aerosol composition (Voisin et al. 2003; Smith et al. 2004; Smith and Rathbone 2008).

Proton-transfer-reaction (PTR) is one form of chemical ionization that has proven to be an effective technique for the measurement of many ambient VOCs (Lindinger at al. 1998; de Gouw and Warneke 2007). Proton transfer from hydronium ions (H_3O^+) is efficient for species with a proton affinity (PA) higher than that of H_2O (691 kJ/mol), including molecules with alcohol, ether, carbonyl, carboxyl, nitrile, amine, or aromatic groups. Since most oxidized organic species, such as those expected to comprise much of the aerosol organic mass fraction, have a higher proton affinity than water, proton transfer chemical ionization using H_3O^+ is expected to be an effective, and relatively soft, form of ionization for these compounds.

We have recently constructed a custom PTR-MS instrument using an aerosol collection/thermal desorption inlet coupled to a quadrupole ion trap mass spectrometer to make rapid (approximately half hour time resolution) measurements of speciated aerosol organic compounds, including semi-volatile species. The primary goal of the instrument is to detect individual aerosol organic species that could serve as markers in order to identify organic aerosol sources and formation and processing mechanisms, including potential semivolatile contributions. This article details the design of the instrument, its characterization in the laboratory, and some results from an initial field deployment aboard a ship in the Houston, Texas, area.

INSTRUMENT DESCRIPTION

The instrument has two major subsystems: an aerosol collection/desorption inlet and a PTR drift tube coupled to an ion trap mass spectrometer. A schematic of the instrument showing both of these subsystems is shown in Figure 1.

Aerosol Collection and Thermal Desorption

Aerosol collection is used to accumulate aerosol mass and provide separation from gas phase organic compounds. Sample air containing aerosols enters the instrument through an inlet nozzle (0.5 mm diameter, 1.05 cm long, $\sim$1.8 L min^{-1} flow under choked conditions). The jet from the nozzle is directed onto a 0.635 cm diameter stainless steel collection target, and particles with diameters greater than the cut point are collected by direct impaction on the target surface. The cut point is determined by the nozzle geometry and particle density. The collection of particles on the target is also likely to be affected by particle morphology. The aerosol collection/desorption chamber, shown in detail in Figure 2, is a stainless steel hexagon with 2.75 inch ConFlat (CF2.75) openings on the top and bottom and six 1.33 inch ConFlat (CF1.33) openings on the sides (Kimball Physics, Inc.). The inlet nozzle extends into the chamber through one CF2.75 flange while the aerosol target is mounted in the other. CF1.33 flanges are used for pumping, flowing carrier gas in and out, and monitoring the chamber pressure. During sampling, the inlet chamber pressure is typically 13 to 27 mbar, depending on ambient pressure and the capacity of the roughing pump used, and is kept low in order to reduce the potential positive artifact (discussed more below) that would arise from adsorption of gas-phase VOCs onto the collection target and chamber surfaces.

To further reduce potential adsorption to the chamber walls during sampling and desorption, the aerosol collection/desorption chamber is maintained at a constant elevated temperature (typically 140°C), while the aerosol target is cooled to near ambient temperature to reduce evaporative losses during sampling. The aerosol target cooling is achieved by flowing

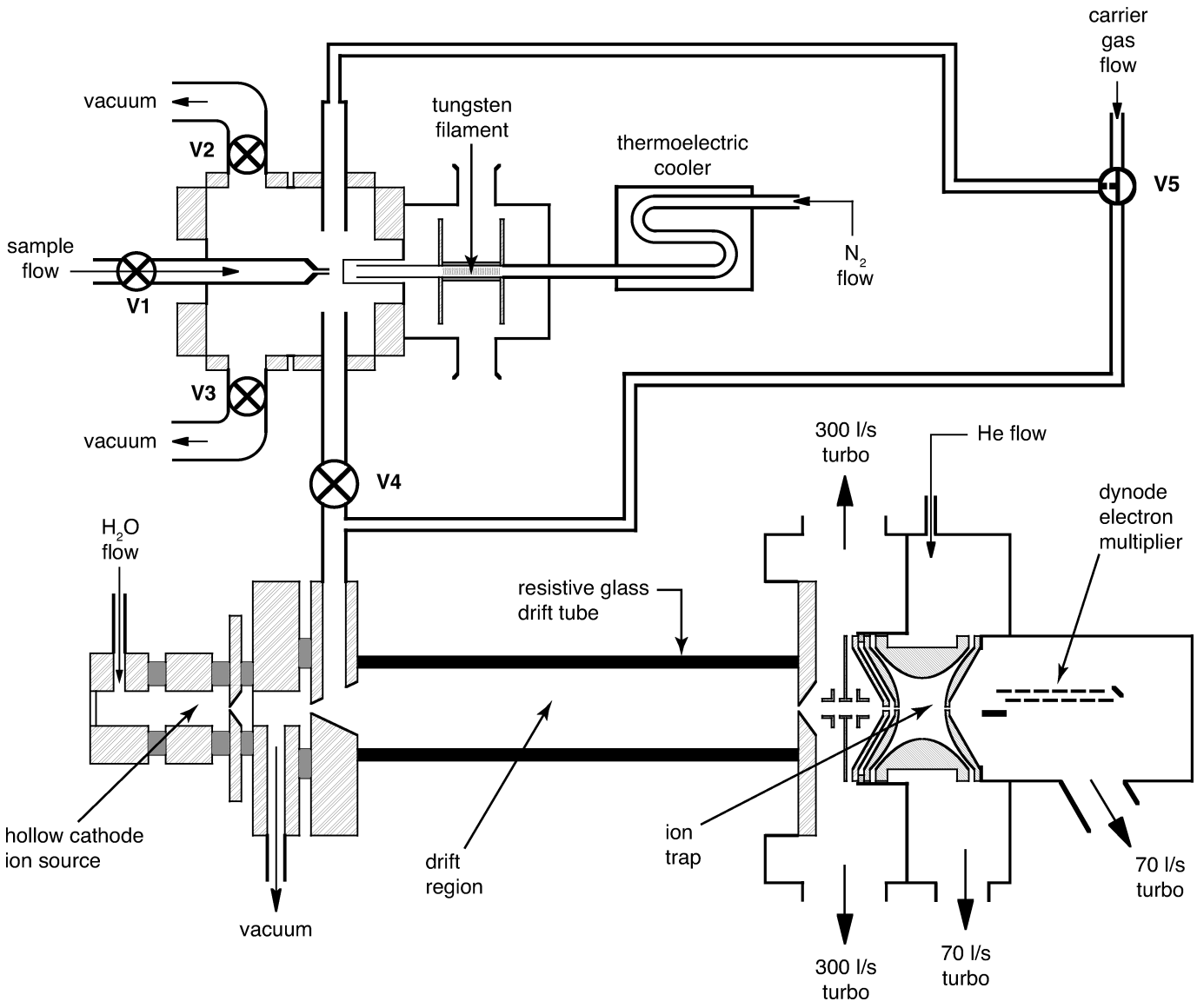

FIG. 1. Schematic of the instrument showing the major components of the aerosol inlet and mass spectrometer.

5 STP L min^{-1} (STP = 273 K, 1 atm) of N_2 through a thermoelectric cooler (TE Technology, Inc. Model LC-035) against the back (air side) of the target. The thermoelectric cooler typically operates at 0–5°C, depending on the room temperature, resulting in an aerosol target temperature during sampling of 25–30°C. To desorb the collected organic compounds, the aerosol target is heated by heating the N_2 flow using a tungsten filament located in the cooling gas stream. The temperature of the aerosol target is regulated by a multiple set-point temperature controller (Love Controls, Model 16A) connected to a silicon-controlled rectifier power controller (Avatar Instruments, Model A1P) that regulates the current through the filament. By this means, the aerosol target temperature is raised from its near-ambient collection value to 150°C within 15 s in order to volatilize the collected aerosol organic compounds as rapidly as possible to shorten the required analysis time and maximize the signal to noise to achieve a lower detection limit.

Volatilized compounds are entrained into a carrier gas flow and transported to the drift tube for ionization and detection. The tubing (stainless steel and alumina ceramic) and valve (Tescom, Magnum 31 series) connecting the collection/desorption chamber to the drift tube are maintained at constant temperatures of 135–145°C to reduce adsorption of volatilized compounds to surfaces during transfer to the drift tube. Experience with prior instrument configurations indicated that the presence of cool sections in the flow path leads to significant tailing of the measured desorption signals.

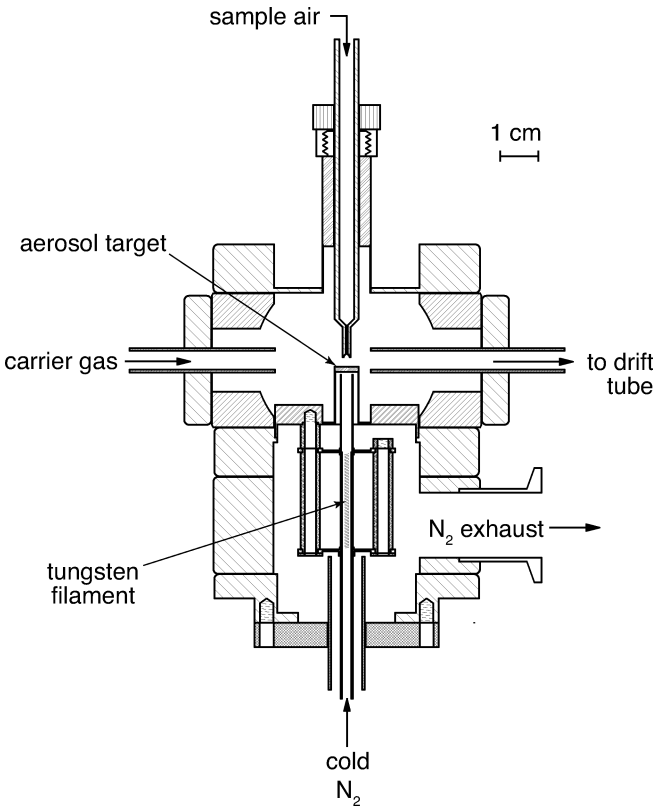

FIG. 2. Schematic of the aerosol collection/desorption inlet chamber showing details of the sample nozzle, aerosol target, and carrier gas inlet and outlet to scale. The vacuum ports are obliquely into and out of the page. The diameter of the nozzle (D_N) is 0.5 mm and the nozzle to target distance (S) is 3 mm ($S/D_N = 6$).

PTR-ITMS

The mass spectrometer consists of a proton-transfer-reaction (PTR) chemical ionization drift tube coupled to a quadrupole ion trap (see Figure 1). The reagent ion source for the drift tube is a hollow cathode discharge in pure water vapor, similar to that previously described by Warneke (2005a) with slight modifications. The water vapor from the source is pumped away by a scroll pump (Varian, Inc., Model IDP-3). A variable vacuum valve (Leybold, Inc.) is used to maintain the pressure in the water vapor pump ring within ± 0.1 mbar of that measured at the drift tube inlet in order to prevent excess water vapor from entering the drift tube while minimizing the amount of sample flow that is diverted from the drift tube. The drift tube used for this instrument is the first reported use of a monolithic resistive glass tube (Burle Industries, Inc.) for PTR-MS. The drift tube is 25 cm in length with an inner diameter of 2.35 cm and a total resistance of 7.8 MΩ. Carrier gas containing the desorbed aerosol organic compounds enters through a port on the side of a steel plate at the upstream end of the drift tube (Figure 1). Ions from the hollow cathode source enter through a 0.6 mm diameter orifice in the center of the plate and react with analyte molecules in the carrier gas as the ions are accelerated to an effective drift velocity by the drift field down the length of the tube. The pressure in the drift tube with a carrier gas flow of 11.25 sccm is 2.1 mbar. The drift tube is heated to 160°C in order to prevent significant adsorption of the volatilized compounds. This elevated temperature and the use of dry N_2 for the carrier gas has the effect of allowing the use of a lower drift field than is commonly used in PTR-MS instruments to prevent excess water clustering with the hydronium and analyte ions. A potential of 850V is applied to the drift tube, producing a drift field of 34 V cm^{-1}, which yields an E/N (E = electric field; N = gas molecule number density) of 95 Townsends (Td). This is somewhat lower than the optimized E/N typical for near-ambient temperature drift tubes of 120 Td (Lindinger et al. 1998; de Gouw and Warneke 2007).

Gas and ions exit the drift tube through a 0.5 mm diameter orifice in the exit plate and enter a vacuum chamber pumped by two 300 L s^{-1} turbomolecular pumps (Varian, Inc., model Turbo-V 301) to a pressure of 7×10^{-4} mbar. A set of four electrostatic lenses focus the ions exiting the drift tube toward the entrance pinhole to the ion trap. The voltage applied to the fourth lens is switched in order to act as a gate to prevent the ion beam from entering the trap during mass scans.

The ion trap used in the instrument is a modified hyperbolic geometry design (Franzen et al. 1995) with radius $r_0 = 1$ cm and axial half-length $z_0 = r_0/\sqrt{1.9} = 0.7255$ cm, similar to that described by Warneke et al. (2005a). The trap is contained in a second vacuum chamber separated from the first by a radial o-ring seal on the outer edge of the spacer between the fourth (gate) electrostatic lens and the entrance endcap of the ion trap. This chamber is pumped by a 70 L s^{-1} turbomolecular pump (Pfeiffer Vacuum, Inc., TMH071P). A 3.4 sccm flow of ultrapure helium is added to the trap chamber to produce a pressure of 1.33×10^{-3} mbar inside the trap. This pressure of helium buffer gas in the trap represents a widely used operational compromise between higher ion trapping efficiency at higher pressure and better mass resolution at lower pressure. A radiofrequency (RF) power supply (RM Jordan Co., Inc., model D-1203) operating at approximately 1.02 MHz and capable of producing a maximum 5000 volts peak-to-peak (V_{p-p}) supplies the RF voltage applied to the ion trap ring to generate the trapping field. Auxiliary voltages generated by an arbitrary waveform board (ZTEC model ZT530PXI) are applied to the endcaps of the trap to serve two functions: (1) a filtered noise field (FNF) is applied to the endcaps during trapping to prevent accumulation of reagent or other unwanted ions that would otherwise overfill the trap, and (2) a 420 kHz sine wave axial modulation of the trapping field is applied during mass scans to improve mass peak resolution and extend the mass range to higher values. Ions are scanned out of the trap using mass selective instability by ramping the amplitude of the trap RF drive voltage and are detected using an off-axis 10 kV dynode discrete electron multiplier (ETP model AF632) and preamplifier. The analog voltage signal from the preamplifier is digitized at 200 kHz (28 samples amu^{-1}) to produce the mass spectrum. The full mass to charge ratio (m/z)

range for the ion trap operating with these parameters is 11 to 403.

An ion trap was chosen for this application due to its ability to rapidly and simultaneously measure the entire mass spectrum. This leads to a multiplex advantage over quadrupole mass filters when a large number of mass to charge ratios need to be measured concurrently, even accounting for the low efficiency (typically ~1%) with which ions are trapped relative to the ion throughput of a quadrupole mass filter.

Instrument Control and Operation

A custom LabVIEW program running on a computer in a PXI chassis (National Instruments, Inc.) controls the switching of valves, setting of voltages and flows, monitoring of temperatures and pressures, and operation of the ion trap. The complete operation of the instrument is automated and capable of running for periods of several days without operator intervention. The elevated temperatures of the aerosol collection/desorption chamber, transfer line and valve, and drift tube are controlled using stand-alone temperature controllers (Omega Engineering, Inc., model CNi3254) that hold the temperatures constant to $\pm$ 1°C.

General operational parameters for the ion trap during analyte ion detection are to trap ions for 1 or 2 seconds with the ring RF amplitude at approximately 450 V_{p-p}. This value results in trapping of ions with m/z greater than 21 and produces optimized trapping efficiency over a broad range of m/z. During trapping, a FNF applied to the trap endcaps is used to destabilize ions with m/z less than 38 in order to avoid overfilling the trap with $H_3O^+ \cdot H_2O$ (m/z 37) reagent ions (which are typically on the order of 10% of H_3O^+), NO^+, O_2^+, and low mass background ions. The trapped ions are then scanned out of the trap by ramping the amplitude of the trap ring RF drive voltage while applying a constant low voltage RF signal at 420 kHz to the trap endcaps. A full analyte mass scan takes 54 milliseconds (scan rate 7000 amu/s). Including the time required to empty the trap and switch voltages, the total time required to perform an analyte scan is 1.14 or 2.14 seconds, yielding a duty cycle of 0.88 or 0.93, respectively. During desorption analyses, the reagent ion signals are monitored by averaging 10 abbreviated reagent ion scans (trap for 15 ms, scan time 38 ms) every 25 analyte scans, resulting in an overall duty cycle of 0.82 or 0.90. During aerosol collection, since this is otherwise idle time for the mass spectrometer, more frequent reagent scans are mixed with analyte scans to monitor the stability of the hollow cathode ion source.

A typical instrument measurement sequence begins with all valves closed, carrier gas bypassing the collection/desorption chamber, and the aerosol target heater set point set to a low value so that no current is flowing through the filament and the target reaches its minimum temperature of 25–30°C. The roughing valves (V2 and V3) are opened to evacuate residual gas in the chamber from the previous measurement cycle. After 45 seconds, the sample valve (V1) is opened to collect a sample. After a collection period, typically 2 to 10 min, the sample valve is closed while the roughing valves remain open to evacuate the chamber for an additional 30 seconds. The roughing valves are then closed and the transfer valve (V4) is opened connecting the inlet chamber to the drift tube, and the 3-way carrier gas valve (V5) is switched to direct the carrier gas through the inlet chamber. After a 15 s delay to allow the drift tube pressure to restabilize, the aerosol target temperature controller set point is switched and the aerosol target is heated to 150°C and held there for 3 to 5 min. The target temperature set point is then switched back to the low value and the target is allowed to cool for 90 s under continued flow. The carrier gas valve is then switched to bypass the collection/desorption chamber and the transfer valve is closed.

The data are processed by identifying peaks within the recorded desorption spectra, integrating the peaks over 1 m/z widths, skipping the initial 3 spectra (while the aerosol target temperature is starting to rise) and then summing the next 50 spectra to calculate a summed desorption signal at each detected mass. The mass spectral data are recorded in analog to digital converter (ADC) units and the integrated peak areas are converted during data reduction into ion counts using the measured single ion area of 0.5 ($\pm$0.2) ADC units.

INSTRUMENT PERFORMANCE

Gas-Phase Sensitivity and Detection Limit

The sensitivity of the instrument to gas-phase organic compounds was determined in order to compare the performance of the mass spectrometer to that previously reported for a gas-phase PTR ion trap mass spectrometer (PIT-MS) (Warneke et al. 2005a; Warneke et al. 2005b). A small flow from a cylinder containing a suite of organic compounds at part per million (ppm) levels in N_2 was added to the carrier gas flow before it entered the inlet chamber and the signals from the VOCs were measured using the instrument. Results indicate sensitivities ranging from 6.5 ions $ppbv^{-1}$ for a 2 s trapping period for acetone at m/z 59 to 0.6 ions $ppbv^{-1}$ for α-pinene at m/z 137. The corresponding 2 s detection limits, defined as 3 times the standard deviation in the background signal (3σ), for these compounds were 1.8 and 2.2 ppbv. The detection limit values for the two compounds are similar in spite of the differences in sensitivity due to the much lower background at m/z 137 relative to m/z 59. Signal averaging to 2 min, such as is typically reported by the PIT-MS or quadrupole based PTR-MS instruments sampling multiple selected masses, yields detection limits of 240 and 295 pptv, respectively. This compares reasonably well with the 2 min detection limits for acetone (200 pptv) and monoterpenes (205 pptv) reported for the PIT-MS instrument (Warneke et al. 2005b). A major reason for the lower sensitivity for α-pinene at m/z 137 is the fact that monoterpenes tend to fragment after ionization, with the dominant fragment appearing at m/z 81. If m/z 81 is used to measure α-pinene, the sensitivity is 4.2 ions $ppbv^{-1}$ and the 2 s and 2 min

detection limits are 1.1 ppbv and 150 pptv. This quantification is possible only if there are no additional species contributing to the signal at m/z 81.

By expressing the gas-phase sensitivity and detection limits in terms of the flux of molecules through the drift tube, these values can be used to estimate the potential signal from collected and desorbed aerosol organic compounds and a theoretical minimum detectable collected mass. A mixing ratio of 1 ppbv in the drift tube corresponds to a flux of about 1×10^{10} analyte molecules per 2 s trapping period. A single scan sensitivity of 2 ions $ppbv^{-1}$ is therefore 1 ion per 5×10^9 analyte molecules. A desorption analysis sums the signal from 50 analyte trapping periods and a typical standard deviation of a background desorption signal is 30 ions. A 3σ detection limit would therefore require 90 ions, or 4.5×10^{11} desorbed analyte molecules. Assuming an analyte with a molecular weight of 150 amu, this estimation yields a theoretical minimum detectable collected amount of 0.11 ng.

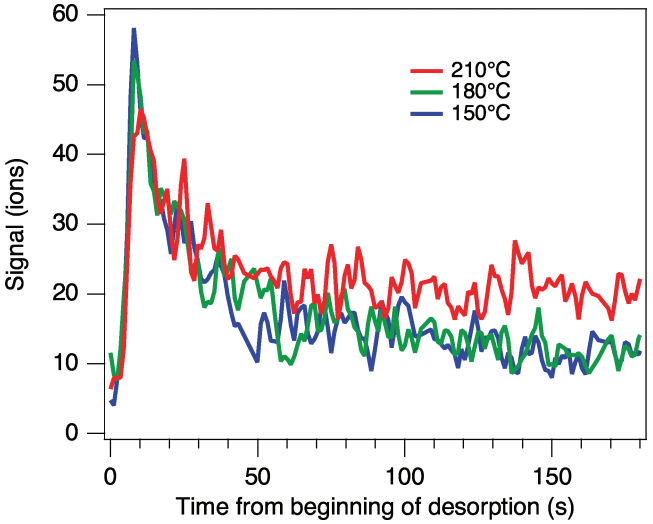

FIG. 3. Glutaric acid signal at m/z 87 during desorptions at 150°C (blue), 180°C (green), and 210°C (red) after sampling similar masses of polydisperse glutaric acid/NH_4NO_3 aerosol.

Aerosol Collection/Desorption Efficiency

The sensitivity of the instrument to aerosol-phase organic species is a convolution of the gas-phase ionization and detection efficiency discussed above with the efficiency with which aerosols are collected in the inlet and then vaporized and transferred to the mass spectrometer. To examine these aspects of instrument performance, we generated 5% and 10% (w/w) glutaric acid/NH_4NO_3 and 5% (w/w) glutaric acid/ NH_4HSO_4 test aerosols using a Collison nebulizer (BGI, Inc. model CN241). Glutaric acid ($C_5H_8O_4$, m.w. 132) was chosen as an experimental analyte because it is a dicarboxylic acid, a class of compound that has been identified in atmospheric aerosols (Finlayson-Pitts and Pitts 2000), and has a high water solubility, making it easy to generate aerosols without the use of organic solvents. The nebulized aerosols were diluted with a flow of dry nitrogen in a 1 L mixing volume to a relative humidity of 7–13%. The 4 to 4.5 L min^{-1} total flow from this volume was passed through a cyclone (URG-2000-30ED), producing a nominal upper cutoff aerodynamic diameter of ~1.2 to 1.5 μm, and then through a differential mobility analyzer (DMA) to select a narrow size range from the polydisperse flow. The output of the DMA was further diluted by N_2 or room air passed through a low pressure drop filter and the flow split to a condensation particle counter (CPC, TSI Inc., Model 3022a) and the sampling inlet of the instrument.

The protonated molecular ion for glutaric acid has a m/z of 133, but no detectable signal was observed at this value. Fragment ions were observed at m/z 115, 87, and 43. m/z 115 represents a loss of H_2O from the protonated molecular ion, and m/z 87 results from an additional loss of CO. m/z 43 is a common fragment from oxygenated organic molecules, CH_3CO^+, and typically exhibits a high background level. m/z 87 was the dominant ion from glutaric acid and is the signal used for analysis of glutaric acid experiments.

For the determination of analyte signal in laboratory experiments, the instrument background in the absence of aerosol was first determined by repeated sampling of filtered room air or nitrogen until stable values were reached across the mass spectrum. This background was then subtracted from the signals measured after sampling aerosols. Background samples were also taken periodically during the course of experiments to test for residual signals arising from incomplete evaporation of samples during desorption. Residual signals above the detection limit for glutaric acid were only observed following large (>10 ng) mass collections.

The desorption temperature of the aerosol target was set to 150°C so that it was only slightly higher than the chamber temperature. Experiments performed to examine the effect of desorption temperature on the analysis of 10% glutaric acid/NH_4NO_3 aerosols indicated that the desorption behavior of the glutaric acid was not improved by operating at higher temperatures. Figure 3 shows the observed signal of glutaric acid at m/z 87 for desorption temperatures of 150°C, 180°C, and 210°C following sampling of similar aerosol mass loadings. The desorption peak does not become sharper with increasing temperature, and the increase in measured total signal summed over the desorption is due to a similar magnitude increase in the background signal at increasing temperature, possibly due to increased desorption or pyrolization of background contamination since similar increases are observed at many m/z in both ambient and background samples.

The 150°C desorption temperature used will limit the compounds that can be measured to those that will evaporate at this temperature in the desorption cycle time of several minutes. An experiment conducted on a prototype instrument found that oleic acid (room temperature vapor pressure $= 2 \times 10^{-8}$ mbar)

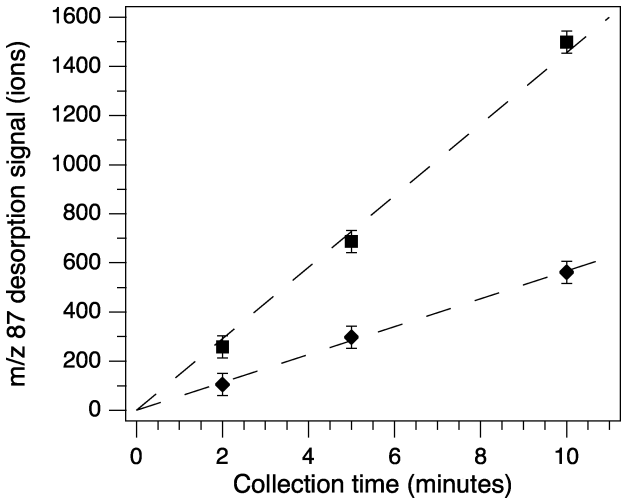

FIG. 4. Integrated glutaric acid desorption signal following collection times of 2, 5, and 10 min of stable aerosol loading at 0.7 (■) and 0.5 (♦) μm (mobility diameter) mixed glutaric acid/NH_4NO_3 particles. The data points represent individual measurements.

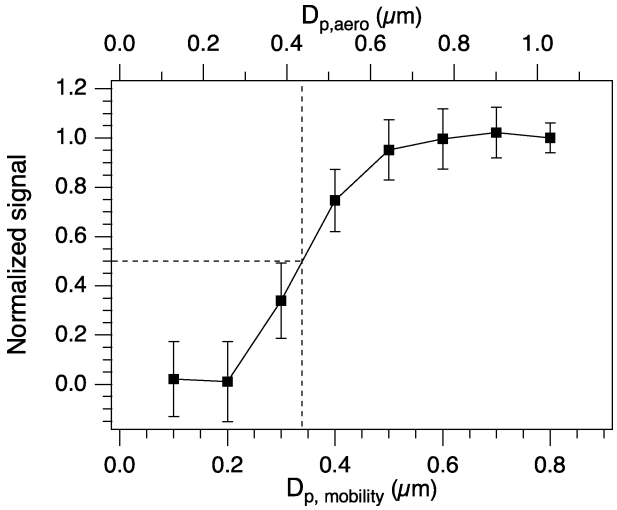

FIG. 5. Normalized signal for glutaric acid from mixed glutaric acid/NH_4NO_3 aerosol as a function of aerosol diameter. The signal at smaller diameters was normalized by assuming 100% efficiency for 0.8 μm particles and dividing the measured signal by the value expected from the mass sampled. The dashed lines indicate the location of the 50% cutoff diameter. The error bars account for the estimated uncertainty in the mass sampled and the removal of the contribution to the measured signal from multiply charged larger particles.

evaporated efficiently at a desorption temperature of 140°C. Based on programmed thermal desorption laboratory studies (e.g., Chattopadhyay and Ziemann 2005; Cappa et al. 2007) organic compounds with room-temperature vapor pressures of 10^{-10} mbar evaporate at temperatures lower than 150°C on the timescale of minutes and should be detectable with the current operational parameters.

To examine the linearity of the instrument response with sampling time, aerosol collections were performed for periods of 2, 5, and 10 min with constant aerosol loading. Figure 4 shows the results for the analysis of glutaric acid/NH_4NO_3 aerosols at two different diameters as a function of collection time. The linearity of the observed signals with time indicates that it is likely that glutaric acid is not being lost at a significant rate during the sample collection period and that sampling for longer periods of time can decrease the ambient mass concentration detection limit for compounds with similar and lower vapor pressures.

The aerosol collection efficiency of the inlet was determined as a function of particle diameter. For this test, the same test aerosol was used and the particle size selected by the DMA was varied from 0.1 to 0.8 μm mobility diameter. The 10% glutaric acid/NH_4NO_3 aerosols at a relative humidity of 10% have an estimated density of 1.66 g cm^{-3} and the DMA selected aerosol diameters translate to aerodynamic diameters of 0.13 to 1.03 μm. An optical particle spectrometer (UHSAS, Droplet Measurement Technologies, Inc.), sampling in parallel with the instrument and the CPC, was used to determine the contribution of multiply charged particles to the aerosol count reported by the CPC and aerosol mass sampled by the instrument. A plot of the normalized signal at m/z 87 is shown as a function of aerosol diameter selected with the DMA in Figure 5. The signal for each selected diameter was normalized by assuming unit collection efficiency for 0.8 μm particles to determine the mass sensitivity and then dividing the measured signal at each size by the expected signal calculated from the aerosol mass sampled. For particle diameters 0.5 μm and below, the contribution to the observed signal from doubly and triply charged larger particles was removed prior to normalizing by subtracting the signal calculated for the observed number of larger particles calculated using their previously determined collection efficiencies. The results of this experiment indicate that the sampling nozzle has a lower aerodynamic 50% cutoff diameter of approximately 0.45 μm, which limits the analysis to larger particles in the accumulation mode and above.

The overall sensitivity of the instrument to glutaric acid in mixed aerosols was examined by sampling a range of total aerosol mass at aerodynamic size ranges above the observed cut-off diameter. Figure 6 shows the instrumental response to 2 min samples of size-selected 5% glutaric acid/NH_4HSO_4 aerosols. The total sampled mass was calculated from the CPC measured particle concentration and the DMA selected diameter. The diameters selected were sufficiently large that the cyclone upstream of the DMA should have removed the doubly charged larger particles that would have made it through the DMA. The sensitivity of the instrument, given by the slope of the orthogonal regression line, is 376 ions per ng sampled. Using three times the observed standard deviation of m/z 87 summed desorption signals while sampling lab air of 27 ions, the glutaric acid detection limit is calculated to be 0.22 ng. This is within a factor of 2 of the detectable mass estimated from the gas-phase sensitivity measurements described above. At the instrument sample flow rate of 1.8 L min^{-1}, a 10-minute sampling period (18 L) would

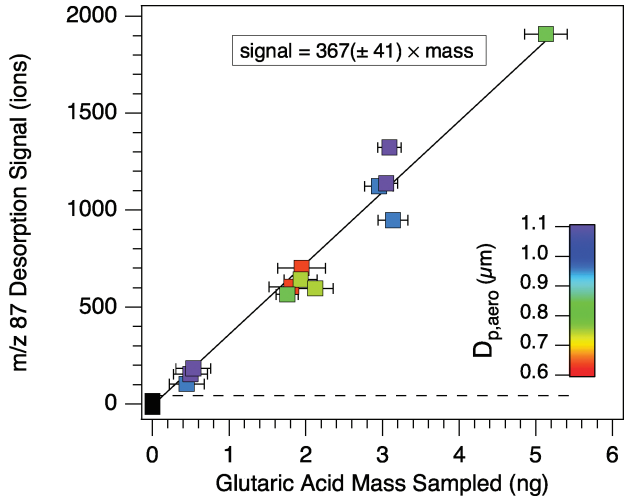

FIG. 6. Sensitivity of the instrument to glutaric acid in 5% (w/w) glutaric acid/NH_4HSO_4 aerosols in the size range 0.6–1.1 μm aerodynamic diameter.

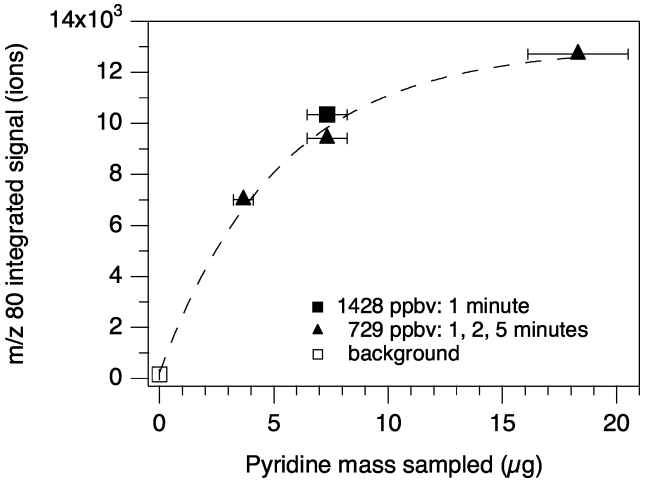

FIG. 7. Observed signal at m/z 80 versus the total mass of gas-phase pyridine sampled. A sample flow mixing ratio of 729 ppbv (▲) was sampled for 1, 2, and 5 min, and a mixing ratio of 1458 ppbv (■) was sampled for 1 min. The dashed line is a guide to the eye through the 729 ppbv data points.

yield a detection limit of 12 ng m^{-3}. Most oxygenated aerosol organic compounds that will volatilize at 150°C or below are likely to have a similar limit of detection.

Sampling Artifacts

Positive artifacts in the measurement could arise from the adsorption of lower volatility gas-phase species onto the collection surface during sampling, and negative artifacts from the premature desorption of aerosol-phase semivolatile species.

The magnitude of the potential positive artifact was investigated by sampling nitrogen containing high mixing ratios of pyridine (vapor pressure ~21 mbar at 20°C). Mixing ratios of 729 or 1458 ppbv, corresponding to 3.66 and 7.33 μg min^{-1}, were sampled by the instrument for periods of 1, 2, and 5 min and the desorption signal measured. Figure 7 shows the observed signal at m/z 80 versus the total mass of pyridine sampled in μg. The observed sensitivity is 0.7 ions per ng pyridine sampled for the 5 min collection. These results indicate that high mixing ratios of lower volatility gas-phase compounds can produce a signal in the instrument during normal operation, but that the sensitivity is quite low, less than 0.2% of that determined for glutaric acid.

The negative artifact that would arise from evaporative loss during sampling or the subsequent pump down of the chamber prior to analysis has not been explicitly studied for semivolatile species, but the results of the experiment with gas-phase pyridine can provide some information. The fall-off of the observed signal with increasing collection time at a constant mixing ratio indicates that some loss is occurring during sampling. Comparing the desorption signal after 2 and 5 min of sampling the 729 ppbv flow with an estimated signal based on the measurement after sampling for 1 min, there were losses of 28% and 60% after the additional 1 and 4 min of sampling. This is likely to be an extreme case due to the volatility of pyridine and that it

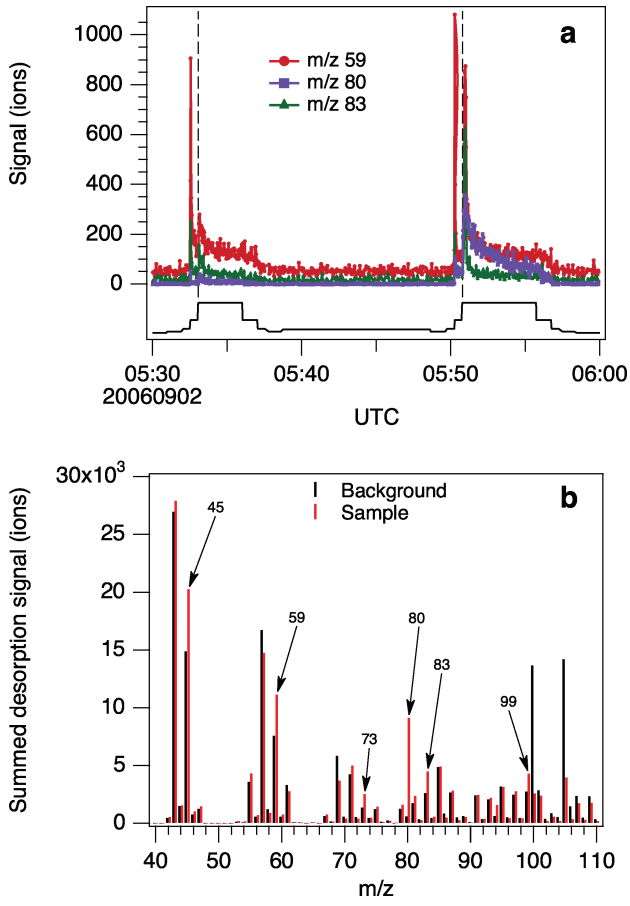

FIG. 8. Background and ambient sample desorptions on September 2, 2006 during TexAQS 2006/GoMACCS. (a) Time series of signals at m/z 59, 80, and 83. The solid black trace indicates the instrument state determined from valve positions and heating status and the vertical dashed lines indicate the initiation of desorption heating. (b) The summed integrated mass spectra for the two (background and sample) desorptions shown in (a). The background spectrum is offset by −0.2 m/z and the sample spectrum by +0.2 m/z.

was being sampled from the gas phase, but indicates that more volatile aerosol phase compounds may be lost during sampling. The linearity of the measured glutaric acid signal with sampling time (Figure 4a) indicates that there is likely to be little loss for lower volatility species.

OPERATION DURING TEXAQS 2006/GOMACCS

The instrument was deployed for ambient sampling aboard NOAA R/V *Ronald H. Brown* during the Texas Air Quality 2006/Gulf of Mexico Atmospheric Composition and Climate Study (TexAQS 2006/GoMACCS), from July 27 to September 11, 2006. On board the ship, the instrument was installed in an ISO container (seatainer) that was mounted on the forward deck along with four other similar seatainers. Measurements with the instrument were made during the period August 13 to September 11.

The goals of the TexAQS 2006/GoMACCS campaign were to investigate factors affecting the air quality in the Houston, TX, area and nearby Gulf of Mexico region and the effects of pollution on regional radiative forcing. To achieve these goals the ship spent time cruising the Houston Shipping Channel and the nearby coastal Gulf of Mexico.

Ambient air for analysis was sampled through the NOAA PMEL sampling mast (Bates et al., 2008) into a different seatainer. The temperature of the sample flows exiting the mast was controlled such that the relative humidity was 60%. Thirty STP L min^{-1} of air was then passed through an impactor with a 50% aerodynamic cut-off diameter of 1 μm and pulled through approximately 12 m of 1.5 cm ID stainless steel tube from which the sample flow for the instrument was drawn. The instrumental flow during sampling was 1.8 L min^{-1} through a 0.34 cm ID stainless steel tube, resulting in approximately isokinetic sampling. The portion of the large diameter sample line within the air-conditioned seatainer and the instrument sample line were heated to 32°C to prevent condensation in the sample lines that would affect particle transmission. The combination of the upstream impactor on the sample line with the aerosol inlet nozzle lower cutoff diameter set the size range of aerosols sampled by the instrument to approximately 0.45–1.0 μm aerodynamic. This size range accounted for 7 to 82% of the submicron aerosol mass with an average value of 28($\pm$13)% over all ambient sample periods based on aerosol number size distribution measurements. The total submicron aerosol mass and fraction within the instrument size range were determined from size resolved aerosol number concentration measurements made using differential mobility particle sizer (DMPS) and aerodynamic particle sizer (TSI, Inc., model 3321) measurements described in Bates et al. (2008).

Due to elevated background signals at a number of masses resulting from outgassing from silicone rubber seals in the roughing valves on the heated collection chamber, the instrument was operated in a mode of alternating 10 min ambient samples and 5 min background samples. This resulted in a measurement interval of 33 min and a sampling duty cycle of 31%. The background samples were collected by not opening the sample valve and closing the roughing valves after evacuating the chamber, allowing outgassed species within the heated chamber to collect on the cooled target. The temperature of the seatainer varied when the air conditioner could not maintain a constant cool temperature, which resulted in a diurnal variation in the observed background signals at some m/z. Background signals measured before and after each ambient measurement were averaged and subtracted from the ambient measurement to produce the ambient signal.

There were several periods during the study when the total aerosol mass in the instrument's sampled size range was less than 1 μg m^{-3} and measurements by an AMS (Bates et al., 2008) indicated that the organic mass fraction was small. During these periods, the closed chamber background spectra closely resembled the ambient sample spectra with the exception of a few masses where the background signals were larger than the ambient samples. We are therefore confident that signals above background at other m/z observed during the study represent real signals.

The reagent ion signals for H_3O^+ and $H_3O^+ \cdot H_2O$ were measured several times during each desorption and average values over the entire cruise were 508 $\pm$ 82 and 100 $\pm$ 48 ions, respectively, for a 15 ms trapping time. The measured analyte signals were normalized to a summed reagent ion signal of 600 ions for each desorption in order to provide a common sensitivity throughout the campaign. Accounting for the measured factor of 3 lower efficiency with which H_3O^+ ions are trapped relative to higher m/z ions (a value similar to the low end of the range of 4–8 reported by Warneke et al. (2005a)), the average total reagent ion signal during the cruise was 108,000 ions s^{-1}. The maximum total analyte ion signal (ions s^{-1}) observed during the study was 13% of the reagent ion signal, and typically less than 8%, indicating that reagent ion depletion was not a significant issue.

Observed Signals

Figure 8a shows the time series for m/z 59, 80, and 83 signals during consecutive background and ambient sample desorptions on September 2 along with a trace indicating the instrument state calculated from valve positions and aerosol target heating. The highest value of the instrument state trace indicates the period when the target is heated and the desorption analysis occurs. The sharp spike that appears in both the background and ambient signals at m/z 59 and m/z 83 prior to the desorption pulse occurs when the carrier gas is first directed through the collection/desorption chamber, transporting residual gases from the chamber into the drift tube. The second spike in the signals is the leading edge of the desorption pulse. The peak in the observed signals typically occurs 12–15 s after the beginning of heating and just as the aerosol target is reaching its 150°C set point, indicating that many organic species are volatilized

rapidly. The m/z 80 signal peaks at the same time as the other signals, but less sharply and with a much longer tail, perhaps indicating a lower volatility or some additional process occurring during desorption. The summed, integrated desorption spectra for the background and ambient sample desorptions appear in Figure 8b. At most masses the signals from the ambient sample are similar to those from the background, but the signals at m/z 45, 59, 73, 80, 83, and 99 are clearly visible above the background. Examples of the elevated background signals due to outgassing from heated components in the inlet chamber are clearly visible at m/z 100 and 105.

To provide a context for the observed signals, we produced an estimate of the non-refractory organic aerosol mass in the 0.45 to 1 μm size range of the instrument. This estimate was calculated by multiplying the organic fraction of the non-refractory submicron aerosol mass measured by an AMS (Bates et al., 2008) with the fraction of total aerosol mass in the sampled size range calculated from the size distribution measurements. This estimate of the sampled organic mass is inexact due to the application of the AMS organic fraction measured from aerosol diameters 0.05 to 1.1 μm to the narrower size range sampled by the instrument, but represents a reasonable proxy for the purposes of this discussion.

Figure 9 shows the time series of several of the signals observed during the second half of the measurement campaign along with a trace of the organic aerosol mass proxy from the AMS in μg m^{-3}. Signals at all m/z except m/z 80 (which exhibited episodes on August 14, 15, and 17 during the first leg of the cruise) were below detection limit prior to August 26. During this period the synoptic flow was predominantly from the south and southeast, bringing relatively clean marine air to the region. On August 26 there was a ~10 h event where signals were observed at m/z 83 and 99, accompanied by small increases in ozone, PAN, and organic aerosol mass measured by the AMS. Signals returned to near or below detection limit until August 30, when the meteorology shifted to more consistent continental flow from the north and northeast and an extended period of active pollution photochemistry ensued. During this period, which lasted until September 9, signals well above detection limit were observed at a number of m/z values from 45 to 153. The largest signal was observed at m/z 83 followed by that at m/z 59.

A list of the m/z at which signals clearly above detection limit were observed during TexAQS 2006/GoMACCS appears in Table 1. Also presented in Table 1 are the maximum signals observed at each m/z, likely ion formulae, and correlations observed between signals where the correlation coefficient, r^2, exceeded 0.52. The strongest observed correlation ($r^2 = 0.68$) was between m/z 59 and 73, which are separated by 14 mass units, a difference that is often indicative of a methyl group. The correlation between most other signal pairs, with the exception of m/z 80, which was uncorrelated with all other signals, was between 0.4 and 0.52. This is due to the common broad increase in the signals that accompanied the increased aerosol mass and photochemical activity during the extended pollution episode, but a lack of consistent correlation on shorter temporal scales. The differences in the signals at the various m/z observed at shorter timescales indicates that significant changes in the composition of the aerosol organic fraction were occurring even during periods when the AMS organic mass remained relatively constant.

m/z 83

This is a relatively low mass ion without an obvious molecular precursor and likely represents a common fragment from higher molecular weight compounds. The possible formulae for a positive m/z 83 ion include $C_6H_{11}^+$, $C_5H_6O{\cdot}H^+$, and $C_4H_6N_2{\cdot}H^+$. The first would be an aliphatic cation fragment of a larger molecule and is not the most likely candidate based on typical fragmentation patterns of organic molecules following proton transfer ionization (Hawthorne and Miller 1986). The nitrogen-containing formula would have a protonated, 5-membered, nitrogen-substituted ring structure, which would have a high proton affinity and be readily ionized in the drift tube. Organic nitrogen compounds have been detected in atmospheric aerosol samples, but the location of the nitrogen atoms within the ring structure and lack of associated oxygen indicate that these compounds, while possible, are not likely to be a significant product of photochemical oxidation. Recent high-resolution time-of-flight AMS measurements in Mexico City yielded organic nitrogen to carbon ratios on the order of 0.02, indicating that nitrogen containing species there likely make only a small contribution to accumulation mode aerosol organic mass (Aiken et al. 2008). The remaining candidate for the observed m/z 83 signal is the oxygen-containing ion. If this were the original molecular ion, the compound would be a methylfuran, pyran, or unsaturated ketone, aldehyde, or alcohol, none of which are expected to contribute significantly to SOA mass. More likely, it is a fragment of a number of larger oxidized molecules. m/z 83 has been observed in the mass spectra of several dicarboxylic acids (including adipic, suberic, and azelaic acids but not glutaric acid) following proton transfer ionization in a recent laboratory study (Cappa et al. 2007) and might represent a tracer for dicarboxylic acid compounds in aerosols.

m/z 59

The signal at m/z 59 is another low mass ion that is likely a common fragment from higher molecular weight compounds. An interesting possibility, however, is suggested by the fact that this is the value at which protonated glyoxal ($C_2H_2O_2{\cdot}H^+$) would be observed. Glyoxal is the smallest α-dicarbonyl and is a product of the photochemical oxidation of aromatic and unsaturated VOCs (Volkamer et al. 2007). It has a vapor pressure of 24 mbar at 20°C, but is soluble in water and known to form hydrates and dimers in solution. Several recent laboratory studies have found that glyoxal is efficiently taken up into aerosols with various compositions (Kroll et al. 2005; Hastings et al. 2005;

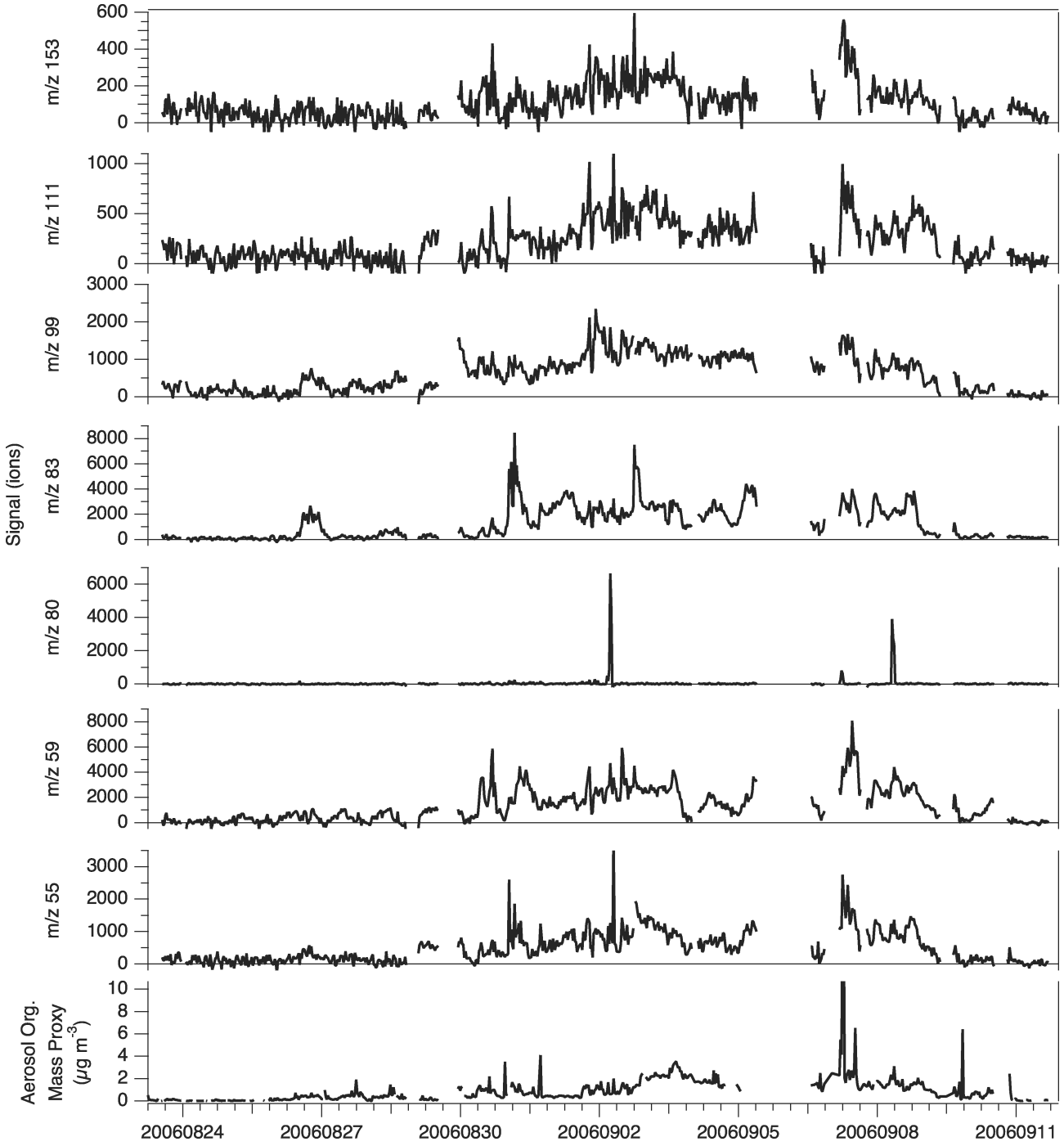

FIG. 9. Time series of several of the observed masses during the second half of the TexAQS 2006/GoMACCS campaign. An estimated organic aerosol mass loading in the 0.45 to 1.0 μm size range determined from aerosol size distribution and AMS measurements is also shown.

Corrigan et al. 2008; Volkamer et al. 2008) and an aerosol loss term has been inferred from measurements of gas-phase glyoxal in Mexico City (Volkamer et al. 2007). A laboratory test sampling the output of a nebulizer containing a glyoxal/NH_4NO_3 aqueous solution indicated that glyoxal does produce a signal at mz/59 in our instrument, although separating the aerosol signal from that of the gas phase was not possible. If the observed m/z 59 signal were glyoxal, it would indicate a potentially significant contribution to the organic aerosol mass from semivolatile species.

TABLE 1
Signals observed during TexAQS 2006/GoMACCS

m/z	Maximum signal value (ions/desorp)	Probable molecular formulas	Correlation with other m/z
45		$C_2H_4O{\cdot}H^+$, CHO_2^+	
55	3676	$C_3H_2O{\cdot}H^+$, $C_4H_7^+$, $(H_2O)_3{\cdot}H^+$	
59	8082	$C_2H_2O_2{\cdot}H^+$, $C_3H_6O{\cdot}H^+$, $C_2H_5ON^+$	73 ($r^2 = 0.68$), 125 ($r^2 = 0.63$)
73	1668	$C_3H_4O_2{\cdot}H^+$, $C_4H_8O{\cdot}H^+$	59 ($r^2 = 0.68$), 125 ($r^2 = 0.61$)
80	6650	$C_5H_5N{\cdot}H^+$, $C_6H_8^+$	
83	8472	$C_5H_6O{\cdot}H^+$, $C_6H_{11}^+$, $C_4H_6N_2{\cdot}H^+$	
97	1566	$C_5H_4O_2{\cdot}H^+$, $C_6H_8O{\cdot}H^+$	
99	2341	$C_5H_6O_2{\cdot}H^+$, $C_6H_{10}O{\cdot}H^+$	
111	1118	$C_6H_6O_2{\cdot}H^+$, $C_7H_{10}O{\cdot}H^+$	113 ($r^2 = 0.60$)
113	808	$C_6H_8O_2{\cdot}H^+$, $C_7H_{12}O{\cdot}H^+$	111 ($r^2 = 0.60$)
125	801	$C_6H_4O_3{\cdot}H^+$, $C_7H_8O_2{\cdot}H^+$, $C_8H_{12}O{\cdot}H^+$	59 ($r^2 = 0.63$), 71 ($r^2 = 0.61$)
139	721	$C_7H_6O_3{\cdot}H^+$, $C_8H_{10}O_2{\cdot}H^+$, $C_9H_{12}O{\cdot}H^+$	
153	594	$C_5H_{12}O_5{\cdot}H^+$, $C_8H_8O_3{\cdot}H^+$, $C_9H_{12}O_2{\cdot}H^+$, $C_{10}H_{16}O{\cdot}H^+$	

m/z 80

The signal at m/z 80 differed from that at other m/z at which signals were observed during the TexAQS 2006/GoMACCS cruise in two significant ways: (1) while the other signals were all at odd m/z values as is expected for protonated ions composed of C, H, and O atoms, m/z 80 is an even mass, which is typically associated with protonated ions from N containing molecules, and (2) instead of broad enhancements during periods of active photochemistry, the signal at m/z 80 was characterized by relatively short duration events (1 to 3 h) above an otherwise flat baseline. This pattern is more suggestive of a primary emission than a photochemical product since the events were discrete and not associated with any typical indicators of photochemical activity such as O_3 or PAN. Individual events did occur coincidently with elevated signals of a number of different hydrocarbons measured during the cruise by GC/MS, including styrene, trimethylbenzenes, propylbenzenes, and in one case acetonitrile, but the overlap was not complete and these compounds all had episodes of elevated levels during which the m/z 80 signal was not observed (J. Gilman, unpublished data). Figure 10 shows that the observed episodes of elevated m/z 80 signal, while separated in time, all occurred in the same location. The ship spent significant time (22% of cruise time, 34% of instrument ambient samples), including 11 nights, sampling in the Barbour's Cut container terminal turning basin in Laporte, TX, at the northwest end of Galveston Bay. An examination of the conditions under which the events were observed reveals that they all occurred at night or in the morning prior to significant break-up of the nocturnal boundary layer, with light local winds (<1 m s^{-1}) from the southwest. There are chemical industries located near the Barbour's Cut terminal, some of which can be seen in the satellite image, that could be the source of the observed signal.

A possible candidate molecule for the m/z 80 signal is pyridine. The pyridine molecule is an aromatic ring with a nitrogen atom substituted for one of the carbons. It has a very high proton affinity (930 kJ mol^{-1}) and is robust, with the molecular ion being the dominant mass peak even after ionization by 70 eV electron impact. Pyridine is used industrially as a solvent and as a feedstock for various chemical products such as pesticides, herbicides, pharmaceuticals, and resins. As was noted above, pyridine has a significant vapor pressure at ambient temperatures ($\sim$31 mb at 27°C) and would not be expected to partition predominantly into the aerosol phase by condensation. However, pyridine is soluble in water and is known to form salts such as pyridinium nitrate (Atkinson et al. 1987), which could lead to significantly increased partitioning into aerosols. Pyridine has previously been observed in particles in the free troposphere (Murphy et al. 2006) and has been identified as the dominant positive core ion in the free troposphere (Eisele 1988; Schulte and Arnold 1990).

DISCUSSION

The goal of the development of the current instrument is the time-resolved, in situ measurement of individual organic compounds in atmospheric aerosols in order to better understand the origins of and processes that lead to the formation of organic aerosol mass. The instrument has demonstrated detection limits for an individual species in laboratory experiments of less than 15 ng m^{-3} for a 10 min sampling period and is capable of making this measurement with a time resolution of better than 20 min. Comparing the current instrument to other instruments recently developed with the goal of making speciated measurements of aerosol organic compounds, the measured detection limit of 0.22 ng sampled mass is an order of magnitude higher than two (TAG and PIAMS) and lower than others (PERCI and ACIMS).

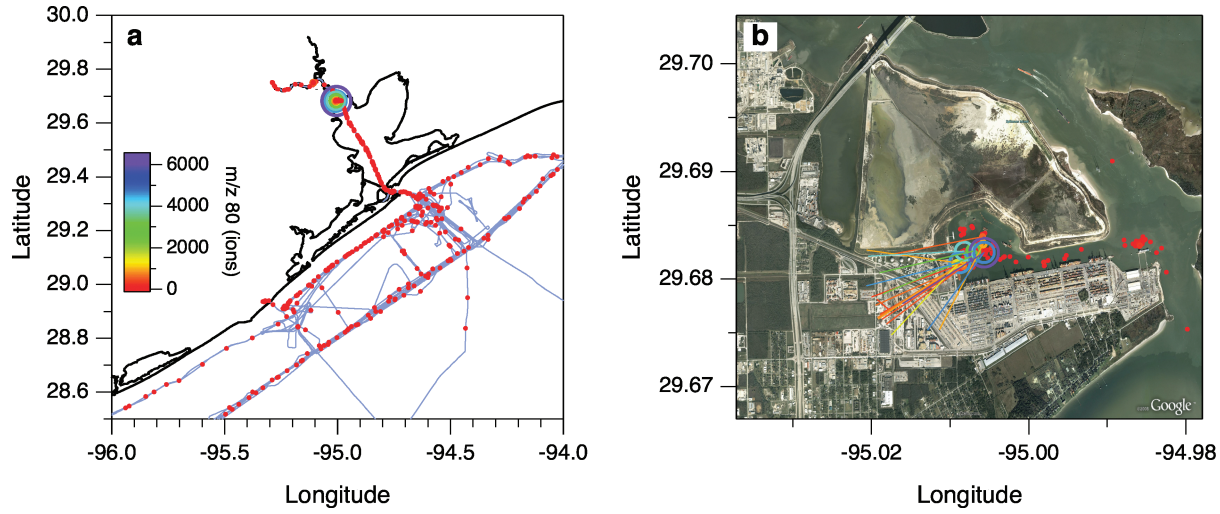

FIG. 10. Location of observed m/z 80 events; (a) map of Galveston Bay, the Houston ship channel and the nearby Gulf of Mexico showing the ship track (light blue) and location of sample measurements colored by the observed m/z 80 signal. The signals are all below detection limit except for a number of samples that were made in the Barbour's Cut container terminal at the northwest end of Galveston Bay. (b) measured m/z 80 signals superimposed on a satellite image of Barbour's Cut (image from Google Earth™) colored by magnitude with wind barbs showing local wind direction for those samples above detection limit.

In their description of the TAG instrument, Williams et al. (2006) reported detection limits ranging from 0.055 to 6.25 ng collected mass based on variety of tested compounds. High sample flow (9 L min^{-1}) for a 30 min collection period yielded a typical detection limit 0.57 ng m^{-3} for an hourly measurement for compounds that transfer efficiently through the collection cell. Gas chromatographic (GC) analysis allows for good speciation of those compounds that pass through the column. However, due to the heating required to evaporate water from the collected sample prior to GC analysis, the instrument is not as well suited to measurement of higher vapor pressure semivolatile species, which are likely to be lost along with the water. The PIAMS instrument (Oktem et al. 2004) achieves detection limits of 5–50 pg collected mass for 1-minute samples of a number of organic compounds. The aerosols are sampled through an aerodynamic lens inlet to high vacuum, resulting in excellent separation of particle and gas phases, but also a significant potential loss of semivolatile species. The PERCI instrument currently has a significantly higher detection limit, 10–100 ng sampled mass (LaFranchi and Petrucci 2006). The authors believe the detection limit can be significantly reduced, but the sampling method will continue to have the same issues with regard to likely evaporation of semivolatile species as the PIAMS. The ACIMS instrument uses proton transfer ionization similarly to our instrument for the detection of organic compounds, but coupled to a quadrupole for mass analysis. While typically used for online measurements in laboratory studies, ambient air measurements have been reported using ACIMS with a sampling inlet that collected aerosol-phase organic compounds by first volatilizing and then condensing them onto the walls of a cooled tube for subsequent desorption and analysis (Hearn and Smith 2006). This method provides a means of measuring both semivolatile and low volatility aerosol organic species. The current reported detection limit for the ACIMS is 4 ng collected mass.

It is apparent from the laboratory studies using glutaric acid as an analyte that while proton-transfer-reaction chemical ionization may be a relatively soft form of ionization compared to electron impact or non-VUV laser ionization, it is still sufficiently energetic to fragment many organic molecules of the types known to contribute to the aerosol organic fraction. Fragmentation is increasingly likely to occur for multifunctional molecules such as those that undergo multiple photooxidation reactions. This fragmentation could potentially be reduced by changing the reagent ions for the chemical ionization to reduce the energetics of the proton transfer reaction by means of introducing an intermediate volatile species such as acetonitrile (PA 779.2 kJ/mol) or ammonia (PA 853.6 kJ/mol) into the water vapor pump region (see Figure 1) at sufficient concentration to convert the $H_3O{\cdot}H^+$ to $R{\cdot}H^+$ prior to entering the drift tube. A similar process was recently reported (Inomata and Tanimoto 2008) to differentiate between isomeric species with different proton affinities. Another possibility would be to convert the instrument to use atmospheric pressure chemical ionization (APCI) to detect the desorbed organic species. Smith and Rathbone (2008) recently reported detection limits of less than 1 pg for dicarboxylic acids in nanoaerosols with the TD-CIMS instrument using APCI that exhibited minimal molecular fragmentation.

There are a number of other ways in which the instrument and its operation could be improved to better address questions of aerosol organic composition and semivolatile partitioning. The

instrument could be easily configured using a multi-port valve to sample ambient air during the aerosol collection period in order to make a complementary gas-phase measurement during what is otherwise mass spectrometer idle time. If this heated whole air measurement were then compared with ambient temperature measurements, additional information on semivolatile species partitioning between the gas and aerosol phases could be revealed. A redesign of the impactor, perhaps using multiple smaller nozzles or a slit nozzle, could lower the cutoff diameter and allow the instrument to sample a larger fraction of the accumulation mode while also increasing the total sample flow, thereby increasing the collected sample mass and reducing the ambient mass loading detection limit for a given collection time. Increasing the desorption temperature to 250 or 300°C would allow detection of lower volatility compounds than are achieved with the current operation. Two capabilities of the ion trap that were not implemented in the first deployment are tandem mass spectrometry (MS-MS) and high resolution. For tandem mass spectrometry, ions of a single m/z can be isolated in the trap and then fragmented using collisionally induced dissociation. The fragmentation patterns could then be used for structure elucidation of commonly observed ions (such as m/z 59) to aid in compound identification (Warneke et al. 2005ab; Steeghs et al. 2007). The ion trap is also capable of high resolution by reducing the mass scan rate, which could be used to distinguish between isobaric ions.

CONCLUSIONS

A new instrument has been developed that uses proton transfer chemical ionization to make measurements of organic compounds present in atmospheric aerosols. Aerosols are collected by direct impaction for a variable time and then rapidly thermally desorbed for analysis using ion trap mass spectrometry. The current inlet impactor collects particles above approximately 0.45 μm aerodynamic diameter. The instrument has demonstrated sensitivity to organic compounds comparable to an existing gas-phase instrument and a laboratory measured detection limit for aerosol-phase glutaric acid of 0.22 ng sampled mass. At the current sample rate of 1.8 L min^{-1} this yields a 12 ng m^{-3} detection limit for a 10-minute sampling time, capable of detecting compounds that comprise on the order of 1% of typical organic aerosol mass loadings. This detection limit is higher than that of two recently reported aerosol organic speciation instruments, but our instrument is potentially better suited for the detection of the potentially significant contribution from semivolatile species to organic aerosol mass.

In its first field deployment, aboard the NOAA R/V *Ronald H. Brown* near Houston, TX, the instrument observed signals at a range of m/z values during periods of photochemical activity and detected the possible presence of pyridine in the aerosol phase, most likely from a primary emission source.

REFERENCES

Aiken, A. C., Decarlo, P. F., Kroll, J. H., Worsnop, D. R., Huffman, J. A., Docherty, K. S., Ulbrich, I. M., Mohr, C., Kimmel, J. R., Sueper, D., Sun, Y., Zhang, Q., Trimborn, A., Northway, M., Ziemann, P. J., Canagaratna, M. R., Onasch, T., Baltensperger, U., and Jimenez, J. L. (2008). O/C and OM/OC Ratios of Primary, Secondary, and Ambient Organic Aerosols with High-Resolution Time-of-Flight Aerosol Mass Spectrometry, *Environ. Sci. Technol.* 42:4478–4485.

Atkinson, R., Tuazon, E. C., Wallington, T. J., Aschmann, S. M., Arey, J., Winer, A. M., and Pitts, J. N. Jr. (1987). Atmospheric Chemistry of Aniline, n,n-Dimethylaniline, Pyridine, 1.3.5-Triazine, and Nitrobenzene, *Environ. Sci. Technol.* 21:64–72.

Bates, T. S., Quinn, P. K., Coffman, D., Schulz, K., Covert, D. S., Johnson, J. E., Williams, E. J., Lerner, B. M., Angevine, W. M., Tucker, S. C., Brewer, W. A., and Stohl, A. (2003). Boundary Layer Aerosol Chemistry During TexAQS/GoMACCS 2006: Insights into Aerosol Sources and Transformation Processes, *J. Geophys. Res.—Atmos.* 113: D00F01, doi: 10.1029/2008JD010023.

Canagaratna, M. R., Jayne, J. T., Jimenez, J. L., Allan, J. D., Alfarra, M. R., Zhang, Q., Onasch, T. B., Drewnick, F., Coe, H., Middlebrook, A., Delia, A., Williams, L. R., Trimborn, A. M., Northway, M. J., DeCarlo, P. F., Kolb, C. E., Davidovits, P., and Worsnop, D. R. (2007). Chemical and Microphysical Characterization of Ambient Aerosols with the Aerodyne Aerosol Mass Spectrometer, *Mass Spec. Rev.* 26:185–222.

Cappa, C. D., Lovejoy, E. R., and Ravishankara, A. R. (2007). Determination of Evaporation Rates and Vapor Pressures of Very Low Volatility Compounds: A Study of the C_4-C_{10} and C_{12} Dicarboxylic Acids, *J. Phys. Chem.* 111:3099–3109.

Chattopadhyay, S., and Ziemann P. J. (2005). Vapor Pressures of Substituted and Unsubstituted Monocarboxylic and Dicarboxylic Acids Measured Using an Improved Thermal Desorption Particle Beam Mass Spectrometry Method, *Aerosol Sci. Technol.* 39:1085–1100, doi: 10.1080/02786820500421547.

Corrigan, A. L., Hanley, S. W., and de Haan, D. O. (2008). Uptake of Glyoxal by Organic and Inorganic Aerosol, *Environ. Sci. Technol.* 42:4428–4433.

de Gouw, J. A., Middlebrook, A. M., Warneke, C., Goldan, P. D., Kuster, W. C., Roberts, J. M., Fehsenfeld, F. C., Worsnop, D. R., Canagaratna, M. R., Pszenny, A. A. P., Keene, W. C., Marchewka, M., Bertman, S. B., and Bates, T. S. (2005). Budget of Organic Carbon in a Polluted Atmosphere: Results from the New England Air Quality Study in 2002, *J. Geophys. Res.—Atmos.* 110: D16305, doi:10.1029/2004JD005623.

de Gouw, J. A., and Warneke, C. (2007). Measurements of Volatile Organic Compounds in the Earth's Atmosphere Using Proton-Transfer-Reaction Mass Spectrometry, *Mass Spec. Rev.* 26:223–257.

de Gouw, J. A., Brock, C. A., Atlas, E. L., Bates, T. S., Fehsenfeld, F. C., Goldan, P. D., Holloway, J. S., Kuster, W. C., Lerner, B. M., Matthew, B. M., Middlebrook, A. M., Onasch, T. B., Peltier, R. E., Quinn, P. K., Senff, C. J., Stohl, A., Sullivan, A. P., Trainer, M., Weber, R. J., and Williams, E. J. (2008). Sources of Particulate Matter in the Northeastern United States in Summer: 1. Direct Emissions and Secondary Formation of Organic Matter in Urban Plumes, *J. Geophys. Res.— Atmos.* 113: D08301, DOI: 10.1029/2007JD009243.

Donahue, N. M., Robinson, A. L., Stanier, C. O., and Pandis, S. N. (2006). Coupled Partitioning, Dilution, and Chemical Aging of Semivolatile Organics, *Environ. Sci. Technol.* 40:2635–2643.

Eisele, F. L. (1988). First Tandem Mass Spectrometric Measurement of Tropospheric Ions, *J. Geophys. Res.* 93(D1):716–724.

Finlayson-Pitts, B. J., and Pitts, J. N. Jr. (2000). *Chemistry of the Upper and Lower Atmosphere*, Academic Press, San Diego, CA, pp. 392–403.

Franzen, J., Gabling, R.-H., Schubert, M., and Wang, Y. (1995). Nonlinear Ion Traps, in *Practical Aspects of Ion Trap Mass Spectrometry Volume I*, R. E. March and J. F. J. Todd, eds., CRC Press, New York, USA, 49–167.

Fuzzi, S., Andreae, M. O., Huebert, B. J., Kulmala, M., Bond, T. C., Boy, M., Doherty, S. J., Guenther, A., Kanakidou, M., Kawamura, K., Kerminen, V.

M., Lohmann, U., Russell, L. M., and Pöschl, U. (2006). Critical Assessment of the Current State of Scientific Knowledge, Terminology, and Research Needs Concerning the Role of Organic Aerosols in the Atmosphere, Climate, And Global Change, *Atmos. Chem. Phys.* 6:2017–2038.

Hastings, W. P., Koehler, C. A., Bailey, E. L., and De Haan, D. O. (2005). Secondary Organic Aerosol Formation by Glyoxal Hydration and Oligomer Formation: Humidity Effects and Equilibrium Shifts During Analysis, *Environ. Sci. Technol.* 39:8728–8735.

Hawthorne, S. B., and Miller, D. J. (1986). Water Chemical Ionization Mass Spectrometry of Aldehydes, Ketones, Esters, and Carboxylic Acids, *Applied Spectroscopy* 40:1200–1211.

Hearn, J. D., and Smith, G. D. (2004). A Chemical Ionization Mass Spectrometry Method for the Online Analysis of Organic Aerosols, *Anal. Chem.* 76:2820–2826.

Hearn, J. D., and Smith, G. D. (2006). Reactions and Mass Spectra of Complex Particles Using Aerosol CIMS, *Int. J. Mass Spec.* 258:95–103.

Huey, L. G. (2007). Measurement of Trace Atmospheric Species by Chemical Ionization Mass Spectrometry: Speciation of Reactive Nitrogen and Future Directions, *Mass Spec. Rev.* 26:166–184.

Inomata, S., and Tanimoto, H. (2008). Differentiation of Isomeric Compounds by Two–Stage Proton Trnasfer Reaction Time–of Flight Mass Spectrometry, *J. Am. Soc. Mass Spec.* 19:325–331, doi:10.1016/j.jasms.2007.11.008.

Jayne, J. T., Leard, D. C., Zhang, X., Davidovits, P., Smith, K. A., Kolb, C. E., and Worsnop, D. R. (2000). Development of an Aerosol Mass Spectrometer for Size and Composition Analysis of Submicron Particles, *Aerosol Sci. Tech.* 33(1):49–70.

Kalberer, M., Paulsen, D., Sax, M., Steinbacher, M., Dommen, J., Prevot, A. S. H., Fisseha, R., Weingartner, E., Frankevich, V., Zenobi, R., and Baltensperger, U. (2004). Identification of Polymers as Major Components of Atmospheric Organic Aerosols, *Science* 303:1659–1662.

Kanakidou, M., Seinfeld, J. H., Pandis, S. N., Barnes, I., Dentener, F. J., Facchini, M. C., Van Dingenen, R., Ervens, B., Nenes, A., Nielsen, C. J., Swietlicki, E., Putaud, J. P., Baalkanski, Y., Fuzzi, S., Horth, J., Moortgat, G. K., Winterhalter, R., Myhre, C. E. L., Tsigaridis, K., Vignati, E., Stephanou, E. G., and Wilson, J. (2005). Organic Aerosol and Global Climate Modeling: A Review, *Atmos. Chem. Phys.* 5:1053–1123.

Kleinman, L. I., Springston, S. R., Daum, P. H., Lee, Y.-N., Nunnermacker, L. J., Senum, G. I., Wang, J., Weinstein-Lloyd, J., Alexander, M. L., Hubbe, J., Ortega, J., Canagaratna, M. R., Jayne, J. (2008). The Time Evolution of Aerosol Composition Over the Mexico City Plateau, *Atmos. Chem. Phys.* 8:1559–1575.

Kroll, J. H., Ng, N. L., Murphy, S. M., Varutbangkul, V., Flagan, R. C., and Seinfeld, J. H. (2005). Chamber Studies of Secondary Organic Aerosol Growth by Reactive Uptake of Simple Carbonyl Compounds, *J. Geophys. Res.—Atmos.* 110:D23207.

Lindinger, W., Hansel, A., and Jordan, A. (1998). On-Line Monitoring of Volatile Organic Compounds at pptv Levels by Means of Proton-Transfer-Reaction Mass Spectrometry (PTR–MS): Medical Applications, Food Control and Environmental Research, *Int. J. Mass Spectrom. Ion Proc.* 173:191–241.

Murphy, D. M., and Thomson, D. S. (1995). Laser Ionization Mass Spectroscopy of Single Aerosol Particles, *Aerosol Sci. Tech*. 22:237–249.

Murphy, D. M. (2005), Something in the Air, *Science* 307:1888–1890.

Murphy, D. M., Cziczo, D. J., Froyd, K. D., Hudson, P. K., Matthew, B. M., Middlebrook, A. M., Peltier, R. E., Sullivan, A., Thomson, D. S., and Weber, R. J. (2006). Single-Particle Mass Spectrometry of Tropospheric Aerosol Particles, *J. Geophys. Res.* 111:D23S32, doi:10.1029/2006JD007340.

Nowak, J. B., Huey, L. G., Eisele, F. L., Tanner, D. J., Mauldin III, R. L., Cantrell, C., Kosciuch, E., and Davis, D. D. (2002). Chemical Ionization Mass Spectrometry Technique for Detection of Dimethylsulfoxide and Ammonia, *J. Geophys. Res.* 107(D18):4363, doi:10.1029/2001JD001058.

Oktem, B., Tolocka, M. P., and Johnston, M. V. (2004). On-Line Analysis of Organic Components in Fine and Ultrafine Particles by Photoionization Aerosol Mass Spectrometry, *Anal. Chem.* 76(2):253–261.

Penner, J. E., Andreae, M., Annegarn, H., Barrie, L., Feichter, J., Hegg, D., Jayaraman, A., Leaitch, R., Murphy, D., Nganga, J., and Pitari, G. (2001). Aerosols, Their Direct and Indirect Effects, in: *Climate Change 2001, the Scientific Basis, Contribution of Working Group I to the Third Assessment Report of the Intergovernmental Panel on Climate Change*, J. T. Houghton, Y. Ding, D. J. Griggs, M. Noguer, P. J. van der Linden, X. Dai, K. Maskell, and C. A. Johnson, eds., Cambridge University Press, Cambridge, United Kingdom and New York, 881 pp.

Robinson, A. L., Donahue, N. M., Shrivastava, M. K., Weitkamp, E. A., Sage, A. M., Grieshop, A. P., Lane, T. E., Pierce, J. R., and Pandis, S. N. (2007). Rethinking Organic Aerosols: Semivolatile Emissions and Photochemical Aging, *Science* 315:1259–1262.

Schulte, P., and Arnold, F. (1990). Pyridinium Ions and Pyridine in the Free Troposphere, *Geophys. Res. Lett.* 17:1077–1080.

Seinfeld, J. H., and Pankow, J. F. (2003). Organic Atmospheric Particulate Matter, *Ann. Rev. Phys. Chem*. 54:121–140.

Slusher, D. L., Huey, L. G., Tanner, D. J., Flocke, F. M., and Roberts, J. M. (2004). A Thermal Dissociation-Chemical Ionization Mass Spectrometry (TD-CIMS) Technique for the Simultaneous Measurement of Peroxyacyl Nitrates And Dintrogen Pentoxide, *J. Geophys. Res.* 109:D19315, doi:10.1029/2004JD004670.

Smith, J. N., Moore, K. F., McMurry, P. H., and Eisele, F. L. (2004). Atmospheric Measurements of Sub-20nm Diameter Particle Chemical Composition by Thermal Desorption Chemical Ionization Mass Spectrometry, *Aerosol Sci. Tech.* 38:100–110, DOI:10.1080/02786820490249036.

Smith, J. N. and G. J. Rathbone (2008). Carboxylic Acid Characterization in Nanoparticles by Thermal Desorption Chemical Ionization Mass Spectrometry, *Int. J. Mass Spectrom*. 274:8–13, doi: 10.1016/j.ijms.2008.04.008.

Steeghs, M. M. L., Crespo, E., and Harren, F. J. M. (2007). Collision Induced Dissociation Study of 10 Monoterpenes for Identification in Trace Gas Measurements Using the Newly Developed Proton-Transfer Reaction Ion Trap Mass Spectrometer, *Int. J. Mass. Spec.* 263:204–212.

Voisin, D., Smith, J. N., Sakurai, H., McMurry, P. H., and Eisele, F. L. (2003). Thermal Desorption Chemical Ionization Mass Spectrometer for Ultrafine Particle Chemical Composition, *Aerosol Sci. Technol.* 37:471–475.

Volkamer, R., Jimenez J. L., San Martini, F., Dzepina, K., Zhang, Q., Salcedo, D., Molina, L. T., Worsnop, D. R., and Molina, M. J. (2006). Secondary Organic Aerosol Formation from Anthropogenic Air Pollution: Rapid and Higher Than Expected, *Geophys. Res. Lett.* 33:L17811.

Volkamer, R., San Martini, F., Molina, L. T., Salcedo, D., Jimenez, J. L., and Molina, M. J. (2007). A Missing Sink for Gas-Phase Glyoxal in Mexico City: Formation of Secondary Organic Aerosol, *Geophys. Res. Lett.* 34:L19807, DOI:10.1029/2007GL030752.

Warneke, C., J. A. de Gouw, E. R. Lovejoy, P. C. Murphy, and W. C. Kuster (2005a). Development of Proton-Transfer Ion Trap-Mass Spectrometry: On-Line Detection and Identification of Volatile Organic Compounds in Air, *J. Am. Soc. Mass Spectrom.* 16:1316–1324, 2005a.

Warneke, C., Kato, S., de Gouw, J. A., Goldan, P. D., Kuster, W. C., Shao, M., Lovejoy, E. R., Fall, R., and Fehsenfeld, F. C. (2005b). Online Volatile Organic Compound Measurements Using a Newly Developed Proton-Transfer Ion-Trap Mass Spectrometry Instrument During New England Air Quality Study—Intercontinental Transport and Chemical Transformation 2004: Performance, Intercomparison, and Compound Identification, *Environ. Sci. Technol.* 39:5390–5397.

Williams, B. J., Goldstein, A. H., Kreisberg, N. M., and Hering, S. V. (2006). An In-Situ Instrument for Speciated Organic Composition of Atmospheric Aerosols: Thermal Desorption Aerosol GC/MS-FID (TAG), *Aerosol Sci. Tech.* 40:627–638.

Williams, J. D., Cox, K. A., Schwartz, J. C., and Cooks, R. G. (1995). High Mass, High Resolution Mass Spectrometry, in *Practical Aspects of Ion Trap Mass Spectrometry Volume II*, R. E. March and J. F. J. Todd, eds., CRC Press, New York, USA, 3–47.

Zhang, Q., Worsnop, D. R., Canagaratna, M. R., and Jimenez, J. L. (2005). Hydrocarbon-Like and Oxygenated Organic Aerosols in Pittsburgh: Insights

into Sources and Processes of Organic Aerosols, *Atmos. Chem. Phys.* 5:3289–3311.

Zhang, Q., Jimenez, J. L., Canagaratna, M. R., Allan, J. D., Coe, H., Ulbrich, I., Alfarra, M. R., Takami, A., Middlebrook, A. M., Sun, Y. L., Dzepina, K., Dunlea, E., Docherty, K., DeCarlo, P. F., Salcedo, D., Onasch, T., Jayne, J. T., Miyoshi, T., Shimono, A., Hatakeyama, S., Takegawa, N., Kondo, Y., Schneider, J., Drewnick, F., Borrmann, S., Weimer, S., Demerjian, K., Williams, P., Bower, K., Bahreini, R., Cottrell, L., Griffin, R. J., Rautiainen, J., Sun, J. Y., Zhang, Y. M., and Worsnop, D. R. (2007). Ubiquity and Dominance of Oxygenated Species in Organic Aerosols in Anthropogenically-influenced Northern Hemisphere Midlatitudes, *Geophys. Res. Lett.* 34:L13801, doi:10.1029/2007GL029979.